Journal of Alloys and Compounds, *176* (1991) 285–293
JAL 0033

Spin-glass-like behaviour of manganese-based amorphous Mn×X alloys (X≡3d, 4d, 5d metals) and its dependence on the Mn–Mn interatomic spacing

Y. Obi and H. Fujimori
Institute for Materials Research, Tohoku University, Sendai 980 (Japan)

K. V. Rao
The Royal Institute of Technology, 100 44 Stockholm (Sweden)

(Received April 24, 1991)

Abstract

The magnetic properties of manganese-based binary amorphous Mn–X alloys have been investigated for the non-magnetic elements X≡3d, 4d, 5d metals. In all the alloys except Mn–Y and Mn–La the magnetization increases monotonically with decreasing temperature and indicates an effective moment for manganese in the range 0.5–1.8 μ_B per manganese atom. From a plot of the effective paramagnetic moment p_{eff} *vs.* the average Mn–Mn interatomic distance D_{nn} we find that spin-glass-like behaviour occurs for $p_{eff} \geqslant 1$ μ_B and $D_{nn} \geqslant 3.0$ Å.

1. Introduction

Manganese-based binary amorphous alloys form an important class of materials for investigating the manifestations of competing magnetic interactions. It is well known that the Mn–Mn exchange interaction depends on the interatomic distance, the exchange integral oscillating in sign with the interatomic distance. Studies on manganese-based binary amorphous alloys reported so far are those in which the local moment is associated only with manganese atoms [1–3], some of which present spin-glass-type characteristics at low temperatures [4, 5]. In manganese-based amorphous alloys consisting of 3d, 4d and 5d metals as the second element, spin-glass-like behaviour is observed only in a few cases, *e.g.* Mn–Y, Mn–La [6] and Mn–Cu–Zr [7].

In this paper we report on our investigations of the magnetic properties of several thick films of amorphous alloys of manganese with non-magnetic 3d, 4d and 5d elements such as scandium, titanium, yttrium, zirconium, niobium, molybdenum, lanthanum, hafnium, tantalum and tungsten. The appearance of spin-glass-like ordering and its relationship to the nearest-neighbour interatomic distance and the observed effective paramagnetic moment are discussed.

0925-8388/91/$3.50

2. Experimental details

Amorphous thick films have been produced by d.c. sputtering on a water-cooled copper substrate from the mother alloy or mixture. In the case of Mn–W the mother alloy was difficult to prepare because the melted material segregated into manganese and tungsten and resulted in a sputtered alloy sample which was tungsten rich and not amorphous. The amorphous alloy films investigated herein had a thickness of about 0.2–0.6 mm. These films have been confirmed to be amorphous using X-ray Fe Kα and/or Cu Kα radiation. The compositions of all the samples were chemically analysed as shown in Table 1 together with several magnetic parameters. The temperature dependence of the d.c. magnetic susceptibility has been measured by a pendulum-type magnetometer and a vibrating sample magnetometer in a magnetic field of 9.5 kOe and a temperature range from 4.2 K to room temperature. The a.c. susceptibility has also been measured by a mutual induction a.c. bridge method in a temperature range from 4.2 to 80 K and an a.c. magnetic field of 4 Oe at a fixed frequency of 400 Hz.

3. Results and discussion

The amorphous phase in the present samples was confirmed by X-ray diffraction from the diffuse peak characteristic of the amorphous state. Results indicate that all the present samples except Mn–Mo and Mn–W were in a single amorphous phase. In the case of Mn–Mo several peaks appeared and the main peak was located near the same position where the characteristic diffuse peak of the other amorphous alloys was found. This is an indication that the short-range Mn–Mo order did not involve a b.c.c. structure but rather involved a closed-packed f.c.c.-like structure. Manganese and molybdenum have about the same atomic radius, therefore Mn–Mo cannot be amorphized easily [8]. In the case of Mn–W, because of the large deviation in sample composition from the intended $Mn_{50}W_{50}$ to a more tungsten-rich composition, the amorphous phase was not obtained. Hauser *et al.* also reported that deposited Mn–W films (composition Mn_9W_{91}) were not amorphous [7].

From the diffuse peak we can estimate the average nearest-neighbour (nn) interatomic distance D_{nn} of the present amorphous alloys by simply assuming a dense random packing structure:

$$D_{nn} = \left(\frac{3}{2}\right)^{1/2} \frac{\lambda}{2 \sin \theta}$$

where λ is the wavelength of X-ray radiation and θ is the diffraction angle. The result is shown in Fig. 1 as a function of the average atomic radius, which is defined as

$$\bar{D} = 2(a_{Mn}R_{Mn} + a_X R_X)$$

TABLE 1

Experimental data obtained for amorphous Mn–X alloys

Element X	Analysed composition (at.%)	Notation	θ (K)	C (10^{-5} erg K Oe^{-2} $mole^{-1}$)	χ_0 (10^{-5} e.m.u. g^{-1})	p_{eff} (μ_B)	Range of data fit (K)
Sc	39.5	$Mn_{60}Sc_{40}$	−15	68.724	0.814	0.683	50–290
Ti	50.9	$Mn_{49}Ti_{51}$	−25	13.190	0.538	0.332	50–290
Y	43.4	$Mn_{57}Y_{43}$	−8.6	156.6	0.724	1.24	50–290
	46.8	$Mn_{53}Y_{47}$					
	51.7	$Mn_{48}Y_{52}$	−8.2	186.5	0.664	1.50	50–290
	63.0	$Mn_{37}Y_{63}$	−6.9	204.7	0.537	1.84	50–290
Zr	52.4	$Mn_{48}Zr_{52}$	−67	44.195	0.455	0.737	50–290
	19.7	$Mn_{80}Zr_{20}$					
Nb	56.0	$Mn_{44}Nb_{56}$	−51	11.389	0.433	0.397	50–290
Mo	50.3	$Mn_{50}Mo_{50}$					
La	37.7	$Mn_{62}La_{38}$	−13.4	75.93	0.596	0.919	50–290
	44.3	$Mn_{56}La_{44}$					
	59.1	$Mn_{41}La_{59}$	−10.5	52.25	0.347	1.033	50–290
	71.4	$Mn_{29}La_{71}$	−7.6	35.70	0.242	1.071	50–290
Hf	61.8	$Mn_{38}Hf_{62}$	−44	12.729	0.202	0.593	50–290
Ta	67.1	$Mn_{33}Ta_{67}$	−14	6.996	0.145	0.486	50–290

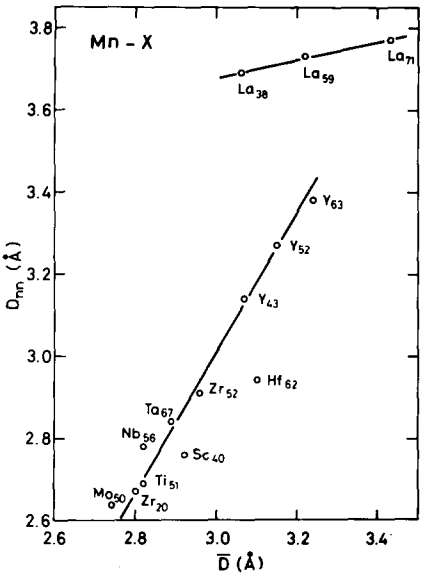

Fig. 1. Relation between average atomic size $\bar{D}$ and average nearest-neighbour distance D_{nn} for the present amorphous alloys.

where a_{Mn} and a_X are the atomic fractions of manganese and X respectively and R_{Mn} and R_X are the atomic radii of manganese and X [9] respectively. This figure also includes D_{nn} of a crystalline Mn–Mo alloy calculated from the main peak of X-ray diffraction for comparison. It is noteworthy to see from this figure that a nearly linear relation between D_{nn} and $\bar{D}$ is obtained in the present series, except for the Mn–La alloys for which there exists a large difference in atomic radii between manganese and lanthanum. This exceptional behaviour could mean that amorphous Mn–La may have a different structure (different type of short-range order) than the other amorphous alloy series investigated by us.

The temperature dependence of the d.c. magnetic susceptibility is shown in Figs. 2(a) and 2(b). The amorphous Mn–Y and Mn–La alloys exhibit an antiferromagnetic or a spin-glass-like behaviour in the low temperature region, with a broad peak in the χ_g *vs.* T curve as shown in Fig. 2(b). Apart from these two alloys, all the other alloys exhibit a monotonic increase in susceptibility with decreasing temperature. This indicates that all the alloys investigated have local magnetic moments and that these local moments arise exclusively from the manganese alone. Hauser and Waszczak also reported that in the amorphous Mn–Zr, Mn–Zr–Cu and Mn–Zr–Ni alloys only the manganese atom has a local moment [2]. The spin glass nature of the Mn–Y and Mn–La alloys is clearly manifested in the a.c. susceptibility *vs.* temperature data shown in Fig. 3. In these χ_{ac} measurements the curves of the Mn–Y and Mn–La alloys display cusps, which is characteristic for spin glass alloys as already reported by us [6]. However, several of the alloys

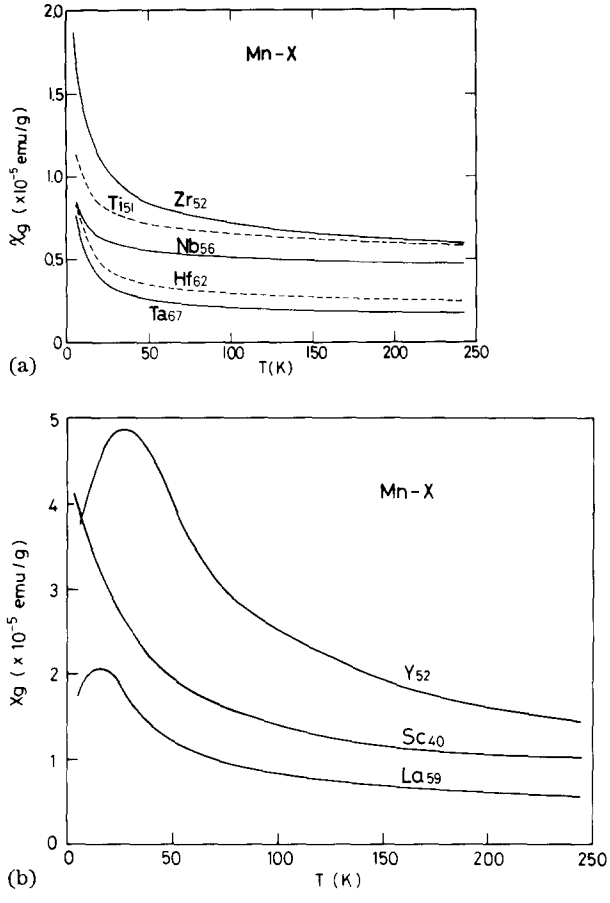

Fig. 2. Temperature dependence of susceptibility obtained with a magnetic field of 9.5 kOe: (a) Mn–(Zr, Ti, Nb, Hf, Ta); (b) Mn–(Y, Sc, La).

investigated ($Mn_{60}Sc_{40}$ and $Mn_{44}Nb_{56}$ are shown as typical examples) do not exhibit any such features down to 4.2 K.

The χ–T curves of all the alloys shown in Fig. 2 can be fitted to the simple Curie–Weiss relation

$$\chi = \chi_0 + \frac{C}{T-\theta}$$

where χ_0 is a temperature-independent susceptibility, C is the Curie constant and θ is the asymptotic Curie temperature. The results of such fits are shown in Figs. 4(a) and 4(b). Several curves give rise to a slight deviation from the straight line fit at low temperatures. This may be ascribed to the occurrence of short-range ferromagnetic or antiferromagnetic ordering between adjacent manganese spins. The parameters obtained from the Curie–Weiss fit are given in Table 1. Note that, as pointed out by Hauser *et al.* [7], the range of temperature considered for the fitting is an important factor because the

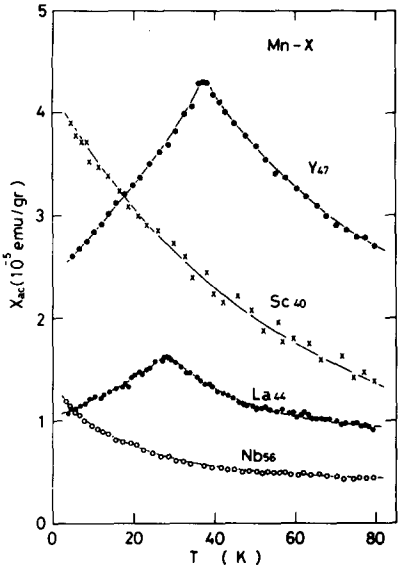

Fig. 3. Typical examples of temperature dependence of a.c. susceptibility measured with an a.c. field of 4 Oe.

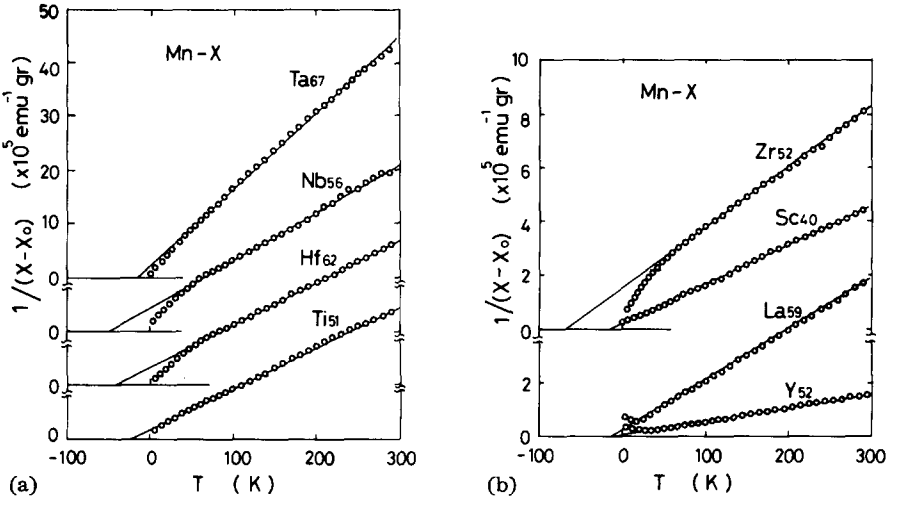

Fig. 4. Temperature dependence of inverse susceptibility for various amorphous alloys investigated: (a) Mn–(Ta, Nb, Hf, Ti); (b) Mn–(Zr, Sc, La, Y). Straight lines are the result of Curie–Weiss fitting.

values of C, θ and χ_0 depend on it. Previously we derived θ and C for the Mn–Zr and Mn–Nb alloys [10] by using the low temperature region (10–200 K) for the fitting. Therefore the parameters C and θ obtained from these fits are subject to errors arising from the relevant short-range ferromagnetic or antiferromagnetic ordering which occurs at low temperatures. This explains

the difference between the values for the parameters deduced in the present paper and those reported earlier [10]. Hauser and Waszczak also reported the result of fitting for amorphous Mn–Zr alloys [2]. Their value of $p_{\mathrm{eff}} \approx 0.87$ μ_{B} is close to the present value of 0.737 μ_{B} for Mn–Zr, but their values of θ and χ_0 are considerably different from our data. The reason is not clear at present. Hauser and Waszczak further demonstrated that the substrate temperature (T_{s}) during sputtering has a rather large influence on these parameters (p_{eff}, θ and χ_0). Therefore the difference in T_{s} between the present experiments ($T_{\mathrm{s}} \approx 300$ K) and their experiments ($T_{\mathrm{s}} \approx 413$ K) may be the reason for the differences mentioned.

From the Curie constant we can calculate the local moment under the assumption that only the manganese atoms contribute. The effective paramagnetic moment per manganese atom is then given by

$$p_{\mathrm{eff}}[\mathrm{Mn}] = C \frac{3k_{\mathrm{B}}}{N\mu_{\mathrm{B}}{}^2} \frac{A}{a_{\mathrm{Mn}}}$$

where k_{B} is Boltzmann's constant, N is Avogadro's constant, μ_{B} is the Bohr magneton and A is the atomic weight. The results are listed in Table 1. A plot of p_{eff} as a function of D_{nn} is shown in Fig. 5. From the figure we can roughly say that p_{eff} of the present series, except for Mn–La, has the same trend, *i.e.* p_{eff} increases with increasing D_{nn}. However, Mn–La behaves differently. The Mn–Mn interaction is usually dependent on the interatomic distance and thus the Mn–Mn distance can account for the magnetic state of the material. For example, $MnPt_3$ is ferromagnetic around an Mn–Mn nearest-neighbour distance of 3.85 Å [11], while MnPt is antiferromagnetic with an Mn–Mn nearest-neighbour distance of about 2.83 Å [12]. In the amorphous case the nearest-neighbour distances have a distribution and therefore one has a mixture of ferromagnetic and antiferromagnetic interactions, giving rise to the so-called spin-glass-like phase. Endo and Ishikawa suggest [13] that the critical Mn–Mn distance making the change from

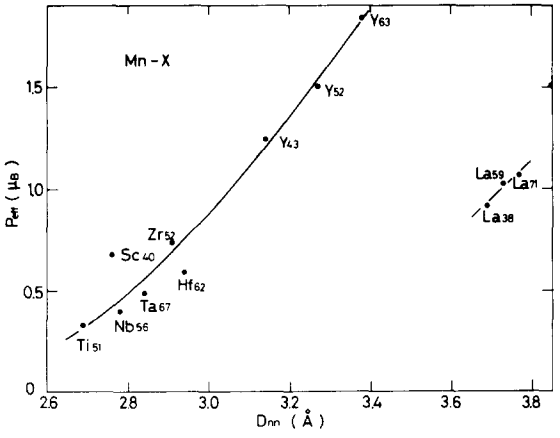

Fig. 5. Relation between p_{eff} and D_{nn} for amorphous alloys investigated in this study.

antiferromagnetic to ferromagnetic interaction is near 3 Å for several manganese-based alloys and compounds. Figure 5 seems to reveal that a spin glass freezing takes place when p_{eff} is larger than about 1 μ_B and D_{nn} is larger than about 3 Å. Obviously the spin-glass-like behaviour in these amorphous Mn–Y and Mn–La alloys, which include fairly high magnetic atom concentrations, arises from the competition of ferromagnetic and antiferromagnetic interactions. On the basis of our results we can roughly say that the threshold of the appearance of the spin glass freezing is $D_{nn} \approx 3$ Å and $p_{eff} \approx 1$ μ_B. Below this critical value of D_{nn} the antiferromagnetic interaction becomes dominant and/or the moment (p_{eff}) may not be large enough to cause random freezing at low temperature.

The above argument is based on our simple analysis. To clarify the origin of the fact that only the amorphous Mn–Y and Mn–La alloys show spin-glass-like behaviour, we need to investigate the properties in more detail. Nevertheless, from the present study we may conclude that our systematic experiments done on the various manganese-based amorphous 3d, 4d and 5d alloys have revealed for the first time various characteristics of the manganese-based binary amorphous alloys. These can be summarized as follows.

(1) Binary amorphous $Mn_{100-x}X_x$ alloys in the vicinity of $40 < x < 60$ (X ≡ Sc, Ti, Y, Zr, Nb, La, Hf, Ta) can be produced by sputtering.

(2) The average nearest-neighbour interatomic distance D_{nn} is nearly linearly related to the average atomic radius for all the amorphous Mn–X alloys except the amorphous Mn–La alloys with low concentrations of lanthanum.

(3) The temperature dependence of the d.c. magnetic susceptibility indicates that the amorphous Mn–Y and Mn–La alloys show spin-glass-like behaviour while the other alloys show simple paramagnetic behaviour. The spin-glass-like nature of the Mn–Y and Mn–La alloys is also clear from the a.c. susceptibility *vs.* temperature curves.

(4) The d.c. susceptibilities at higher temperatures for the present amorphous alloys can be described by the Curie–Weiss law if a temperature-independent term is subtracted.

(5) The effective paramagnetic moments p_{eff} obtained for all the amorphous alloys investigated except Mn–La lie on a common line when plotted as a function of D_{nn}. The paramagnetic alloys are located in the region $p_{eff} < 1.0$ μ_B and $D_{nn} < 3$ Å on this common line, while the spin-glass-like Mn–Y and Mn–La alloys are found in the region $p_{eff} > 1.0$ μ_B and $D_{nn} > 3$ Å.

References

1 T. Mizoguchi and T. Kudo, *AIP Conf. Proc., 29* (1975) 167.
2 J. J. Hauser and J. V. Waszczak, *Phys. Rev. B, 30* (1984) 2898.
3 J. J. Hauser, H. S. Chen and J. V. Waszczak, *Phys. Rev. B, 33* (1986) 3577.
4 J. J. Hauser, *Phys. Rev. B, 22* (1980) 2554.
5 K. Shirakawa, K. Fukamichi, S. Abe, K. Aoki and T. Masumoto, *Sci. Rep. RITU A, 32* (1985) 168.

6 Y. Obi, S. Kondo, H. Morita and H. Fujimori, *J. Phys. (Paris), Colloq. C8, 49* (1988) 1097.
7 J. J. Hauser, J. V. Waszczak, R. J. Felder and S. M. Vincent, *Phys. Rev. B, 32* (1985) 7315.
8 T. Egami and Y. Waseda, *J. Non-Cryst. Solids, 64* (1984) 113.
9 *Table of Periodic Properties of the Elements*, Sergent-Welch.
10 Y. Obi, H. Morita and H. Fujimori, *Appl. Phys. A, 42* (1987) 201.
11 S. J. Pickart and R. Nathans, *J. Appl. Phys., 33* (1962) 1336.
12 J. S. Kouvel, C. C. Hartlius and L. M. Osika, *J. Appl. Phys., 34* (1963) 1095.
13 Y. Endo and Y. Ishikawa, *Solid State Phys., 5* (1970) 245.